THE JOURNAL OF BIOLOGICAL CHEMISTRY
Vol. 279, No. 13, Issue of March 26, pp. 12598–12604, 2004

Printed in U.S.A.

Identification and Characterization of a Glycosaminoglycan Recognition Element of the C Chemokine Lymphotactin*

Received for publication, October 23, 2003, and in revised form, December 22, 2003
Published, JBC Papers in Press, January 5, 2004, DOI 10.1074/jbc.M311633200

Francis C. Peterson‡, E. Sonay Elgin§, Timothy J. Nelson‡, Fuming Zhang¶, Theresa J. Hoeger‡, Robert J. Linhardt¶, and Brian F. Volkman‡‖

From the ‡Department of Biochemistry, Medical College of Wisconsin, Milwaukee, Wisconsin 53226, the §Kimya Bölümü, Mugla Üniversitesi, Mugla 48000, Turkey, and the ¶Departments of Chemistry, Chemical and Biological Engineering, and Biology, Rensselaer Polytechnic Institute, Troy, New York 12180

Chemokine-mediated recruitment of leukocytes *in vivo* depends on interactions with cell surface glycosaminoglycans. Lymphotactin, the unique member of the "C" chemokine subclass, is a highly basic protein that binds heparin, a glycosaminoglycan, with high affinity (~10 nM). We detected lymphotactin-heparin binding by NMR and mapped this interaction to a narrow surface that wraps around the protein. Substitutions in and around this binding site and surface plasmon resonance analysis of heparin binding affinity identified two arginine residues of lymphotactin as critical for glycosaminoglycan binding. Both arginine mutant proteins and the combined double mutant had dramatically diminished *in vivo* activity in a leukocyte recruitment assay, suggesting that the lymphotactin-glycosaminoglycan interactions detected *in vitro* are important for the function of this chemokine. Our results demonstrate that like other chemokines, lymphotactin utilizes highly specific glycosaminoglycan-binding sites that represent potential targets for drug development.

A family of small secreted proteins, chemokines recruit leukocytes from the circulatory system to mediate inflammatory responses in host defense and wound healing (1), control angiogenesis, and regulate lymphoid development (2, 3). Chemokine sequences are divided into four subfamilies, based on the number and spacing of conserved cysteine residues. Many chemokine structures are known, and members of all four subfamilies adopt a canonical tertiary fold, typically stabilized by a pair of disulfide bonds (4); some also form homodimeric structures (5). Chemokines stimulate leukocyte migration by activating specific G protein-coupled receptors expressed in their target cell populations (3, 6). This signaling network of roughly 50 chemokines and 20 receptors is both selective and redundant: specific leukocyte types express a particular receptor and are recruited only in response to their cognate chemokines, however, many receptors can be activated by more than one chemokine ligand (7).

Human lymphotactin (hLtn/XCL1)[1] recruits T lymphocytes and natural killer cells through its specific receptor XCR1 in normal immune function and chronic inflammatory conditions (8, 9). For example, an inappropriate or uncontrolled T cell infiltration driven by hLtn expression is a factor in both Crohn's disease (10) and rheumatoid arthritis (11). Interestingly, the unique ability of hLtn to specifically chemoattract lymphocytes has been exploited therapeutically in combination with the T cell-activating cytokine interleukin-2 (IL-2). T cells recruited by hLtn and activated by IL-2 generated potent antitumor immunity in human clinical trials for treatment of neuroblastoma, where studies with either hLtn or IL-2 alone failed to generate a significant response (12). Hence, hLtn and its analogs with activity toward XCR1 will be extremely valuable as agents for T cell recruitment in cancer vaccines (6), whereas specific antagonists of hLtn activity may be useful for treating certain autoimmune or inflammatory diseases (7).

Protein-glycosaminoglycan (GAG) interactions are essential for *in vivo* signaling by the chemokine network of the immune system (13–15). High affinity chemokine binding to cell surface GAGs is thought to serve in the formation of a concentration gradient leading back to the site of chemokine production. These interactions may regulate the types of chemokines immobilized at inflammatory sites, because the content and composition of cell surface glycosaminoglycans vary with the type and location of endothelial tissues (13).

Mutagenesis studies on a number of CC and CXC chemokines, including RANTES, MIP-1α, MIP-1β, MCP-1, IL-8, SDF-1, and IP-10 identified groups of basic residues responsible for GAG binding (16–24). Whereas a cluster of basic residues commonly associated with heparin-binding proteins (the BB*X*B motif (25)) appears in the 40's loop of the CC chemokines RANTES, MIP-1α, and MIP-1β, GAG binding sites identified in other chemokines are highly divergent (26). Cell-based *in vitro* assays for chemotaxis (or Ca^{2+}-flux) showed that GAG binding mutants of RANTES, MIP-1α, and MIP-1β remained fully functional, suggesting that G protein-coupled receptor binding and activation is independent of the interactions with extracellular matrix (20, 24, 27). However, the same mutants with disrupted GAG binding sites were nonfunctional *in vivo*, demonstrating that the biological activity of chemokines depends on both types of intermolecular interactions (27).

Three-dimensional structures are available for many chemokines, but no chemokine-GAG complexes have been determined. A co-crystal structure is available for heparin bound to the cytokine basic fibroblast growth factor (28), but the features governing protein-GAG recognition are still relatively uncharacterized. Complete description of a functional chemokine signaling complex will require structural characterization of GAG binding elements that represent targets for development of specific chemokine antagonists (14, 29). Like most

* The costs of publication of this article were defrayed in part by the payment of page charges. This article must therefore be hereby marked "*advertisement*" in accordance with 18 U.S.C. Section 1734 solely to indicate this fact.

‖ To whom correspondence should be addressed. Tel.: 414-456-8400; Fax: 414-456-6510; E-mail: bvolkman@mcw.edu.

[1] The abbreviations used are: hLtn, human lymphotactin; IL, interleukin; GAG, glycosaminoglycan; RANTES, regulated on activation normal T cell expressed and secreted; MIP, macrophage inflammatory protein; SDF-1, stromal cell-derived factor 1; MCP, monocyte chemoattractant protein; IP, interferon-γ-inducible protein.

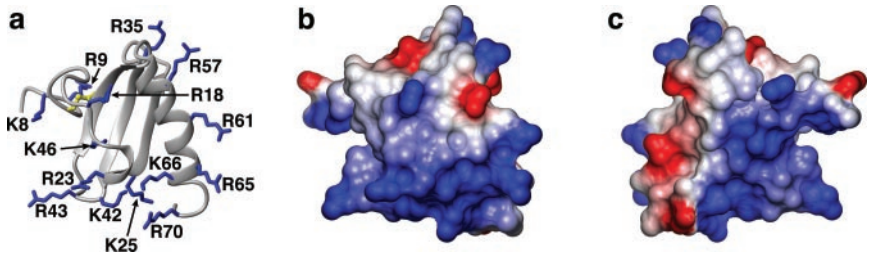

FIG. 1. **hLtn is a highly basic protein.** *a*, ribbon diagram of hLtn with side chains of basic residues shown in *blue* (Protein Data Bank code 1J9O). *b*, surface representation of hLtn oriented as in the ribbon diagram, and colored according to electrostatic potential (calculated in MOLMOL (44)) with positive and negative regions in *blue* and *red*, respectively. *c*, electrostatic surface as in *b* rotated by 180° about the vertical axis. Residues of the unstructured C terminus (71–93) are omitted for clarity.

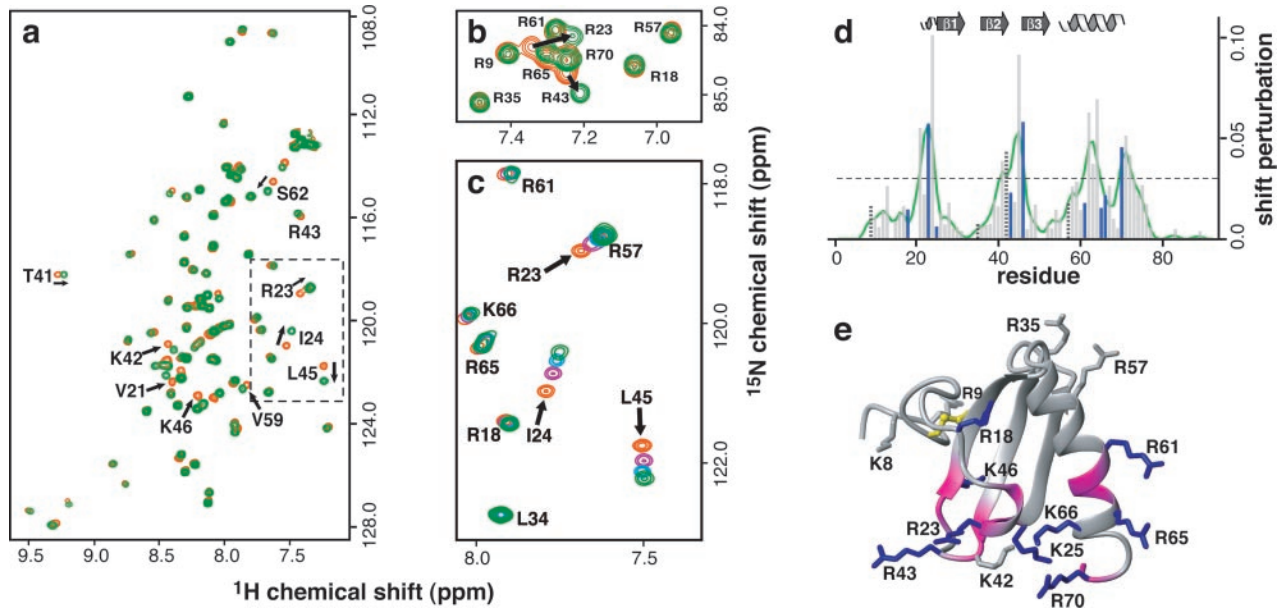

FIG. 2. **NMR identification of an hLtn-heparin binding site.** *a*, two-dimensional ^{1}H-^{15}N HSQC spectra of wild-type hLtn (125 μM) in the presence (*green contours*) and absence (*orange contours*) of a 3-fold molar excess of synthetic heparin pentasaccharide. Each spectrum was acquired at 10 °C, in 20 mM sodium phosphate (pH 6), 200 mM NaCl. *b*, arginine side chain NH signals from HSQC spectra of hLtn with *arrows* highlighting the selective perturbation of Arg-23 and Arg-43 in response to pentasaccharide binding. *c*, titration of hLtn with pentasaccharide shifts a unique set of resonances in a concentration-dependent manner. *Orange*, *magenta*, *blue*, and *green* contours correspond to 0, 125, 250, and 375 μM heparin. *d*, combined backbone ^{1}H and ^{15}N chemical shift perturbations were calculated using the equation: $\Delta\delta_{comb} = [((\Delta\delta^{1}HN)^2 + (0.23{\cdot}\Delta\delta^{15}N)^2)/2]^{1/2}$ and plotted as a function of residue number (45, 46). A threshold of 0.035 was obtained from the mean plus 1 S.D. for shift perturbations of all residues (*dashed line*). Lysine and arginine residues analyzed by mutagenesis are highlighted (*blue bars*). Other basic residues are indicated with *dashed bars*. Smoothed shift perturbations were calculated using a 2-residue moving average $[\Delta\delta_{ave(i)} = (\Delta\delta_{comb(i)} + \Delta\delta_{comb(i+1)})/2]$ (*green line*). *e*, ribbon diagram of hLtn (Protein Data Bank code 1J9O) showing the location of a heparin binding surface. Segments of the backbone with chemical shift perturbations greater than 0.035 are shown in *magenta*. Basic side chains shown in *blue* were selected for mutagenesis, whereas those shown in *gray* were not. Residues of the unstructured C terminus (71–93) are omitted for clarity.

chemokines, hLtn is highly basic and binds heparin with high affinity (~10 nM), presumably through some combination of its 15 lysine and arginine residues (Fig. 1) (13). In this work, we monitored the interaction between ^{15}N hLtn and a synthetic heparin pentasaccharide by NMR spectroscopy. Chemical shift perturbations clearly identified a GAG recognition element involving a subset of basic residues. On this basis, we generated mutant proteins with greatly reduced affinity for heparin, and showed that these substitutions eliminated *in vivo* hLtn activity. Our results identify a specific GAG binding site for the chemokine lymphotactin and suggest that the interaction is essential for *in vivo* function.

MATERIALS AND METHODS

Cloning and Mutagenesis—We previously described the production of human Ltn (hLtn) in *Escherichia coli* using a codon-optimized synthetic gene incorporated into a fusion protein construct with a Factor Xa cleavage site (4). A disadvantage of this approach resulted from Factor Xa proteolysis at a favorable secondary cleavage site in the hLtn sequence, lowering the overall yield of hLtn. In this work we developed an improved method for expression of recombinant hLtn based on the pQE vector system. PCR was used to generate a full-length, codon-optimized hLtn fragment with BamHI and HindIII sites at the 5′ and 3′ ends, respectively, to facilitate insertion into a modified pQE30 vector (Qiagen, Valencia, CA). Modifications to the pQE30 vector include extension of the $(His)_6$ tag to a total of 8 histidine residues and incorporation of a tobacco etch virus protease (30) site as a means of removing the affinity tag. Many chemokines are inactivated by N-terminal modifications, however, lymphotactin containing an N-terminal FLAG epitope was active (31), and deletion of the N-terminal Val residue yielded a functional hLtn protein (32). To accommodate the tobacco etch virus protease recognition sequence, Val-1 was excluded from the expression construct resulting in a recombinant protein composed of residues 2–93 of hLtn (GenBank™ accession U23772). This recombinant hLtn (2–93) protein is referred to as wild-type hLtn throughout this paper.

Site-directed mutagenesis was performed using pairs of complementary primers and the QuikChange kit (Stratagene, La Jolla, CA). All expression vectors were verified by DNA sequencing.

Protein Expression, Purification, and Refolding—The hLtn expression plasmid, pQE308HT-hLtn, was transformed into *E. coli* strain SG13009[pRPEP4] (Qiagen). Cell were grown at 37 °C in LB media containing 150 μg/ml ampicillin and 50 μg/ml kanamycin until the cell density reached A_{600} = 0.7–1.0. Protein expression was then induced by the addition of isopropyl-β-D-thiogalactopyranoside to a final concentration of 1 mM. Following induction, cells were grown for another 3.5 h, harvested and stored at −80 °C until processed further. For uniform

labeling with ^{15}N, cells were grown in M9 media containing ^{15}N-ammonium chloride as the sole nitrogen source.

Recombinant hLtn was found exclusively in the insoluble fraction of the harvested cells, and isolated by the following procedure for purification and refolding. Cell paste from a 1–2-liter culture was resuspended in 10 ml of lysis buffer (50 mM sodium phosphate, pH 7.4, 300 mM NaCl, 10 mM imidizole, 0.1% (v/v) 2-mercaptoethanol, 1 mM phenylmethylsufonyl fluoride) and lysed by two passes through a French pressure cell. Inclusion bodies were isolated by centrifugation at 10,000 × *g* for 15 min at 4 °C, resuspended in 10 ml of solubilization buffer (6 M guanidinium chloride, 50 mM sodium phosphate, pH 8.0, 300 mM NaCl, 10 mM imidizole, 0.1% (v/v) 2-mercaptoethanol), disaggregated by passage through a 16-gauge needle, and clarified by centrifugation at 10,000 × *g* for 10 min. This protein solution was incubated with Ni^{2+}-nitrilotriacetic acid resin (Qiagen) in batch mode for 30 min at room temperature, packed into a 5-ml disposable column, and washed with 3 × 10-ml portions of solubilization buffer. Bound Ltn was eluted with 3 × 10-ml portions of elution buffer (6 M guanidinium chloride, 100 mM sodium acetate, pH 4.5, 300 mM NaCl, 10 mM imidizole, 0.1% (v/v) 2-mercaptoethanol). Eluted fractions were pooled and dialyzed against 3 × 4 liters of 0.3% (v/v) acetic acid to remove denaturant. Separation of the affinity tag was performed by adjusting the buffer conditions to 50 mM sodium phosphate, pH 6.5, 50 mM NaCl, and 0.1% 2-mercaptoethanol, addition of a catalytic amount of tobacco etch virus protease (~1,000:1), and incubation for 3 h at 22 °C. Formation of the single hLtn disulfide was accomplished by dropwise addition of the cleavage reaction into 150 ml of oxidation buffer (20 mM Tris, pH 8.0, 200 mM NaCl), followed by dialysis of the oxidation reaction against 4 liters of oxidation buffer. Oxidized hLtn was concentrated to 20 ml by ultrafiltration in an Amicon stirred-cell using a 3-kDa molecular mass cutoff membrane. Fully refolded hLtn was separated from reduced or aggregated species by reversed-phased high performance liquid chromatography. Purity and identity of all hLtn variants were confirmed by matrix-assisted laser desorption ionization mass spectrometry.

SPR Measurements—Sensor chips (SA, C1, and CM5), 1-ethyl-3-(3-dimethylaminopropyl)-carbodiimide, and *N*-hydroxysuccinimide were from Biacore (Biosensor AB, Uppsala). Semi-purified heparin, heparin-albumin, and heparin-biotin were from Sigma. SPR measurements were performed on a BIAcore 3000 operated using BIAevaluation 3.1 software. Freshly prepared, degassed buffers were used, and all protein samples were purified to >95% by high performance liquid chromatography and filtered. Covalent immobilization was used to avoid baseline drift because of a decaying surface. Reference surfaces were created using the same coupling reagents and carrier agents as the measurement surface, and a reference sensorgram was subtracted from each dataset. Each injection was performed in duplicate, and stringent surface regeneration (2 M NaCl, followed by glycine (pH 2.0) and NaOH (pH 10.0)) was performed between all injections.

Initial SPR studies using biotinylated heparin immobilized on a streptavidin sensor chip failed because of nonspecific binding of hLtn to the surface. Preliminary experiments were performed at 25 °C in 20 mM sodium phosphate buffer (pH 6), using soluble semi-purified heparin (average molecular mass of 11,000 Da). hLtn was covalently coupled through its primary amino groups to a CM5 (carboxymethyl dextran) sensor chip using standard *N*-hydroxysuccinimide ester/carbodiimide coupling chemistry. To identify suitable oligosaccharides for NMR analysis of a hLtn-GAG complex, we also measured the interaction of immobilized hLtn with several homogeneous heparin fragments purified from porcine mucosal heparin (33, 34). Sensorgrams were acquired at 25 °C in 20 mM sodium phosphate buffer (pH 6) for a panel of seven heparin oligosaccharides with the general formula ΔUA2S (1[→4)-α-D-GlcNS6S(1→4)-α-L-IdoA2S(1→]$_n$4)-α-D-GlcNS6S, where ΔUA is 4-deoxy-α-L-*threo*-hex-4-eno-pyranosyluronic acid, GlcN is 2-deoxy-2-aminoglucopyranose, IdoA is idopyranosyluronic acid, S is sulfate, and $n = 1$ (tetrasaccharide); $n = 2$ (hexasaccharide); $n = 3$ (octasaccharide; $n = 4$ (decasaccharide); $n = 5$ (dodecasaccharide); $n = 6$ (tetradecasaccharide), or $n = 9$ (ecosisaccharide).

To provide an efficient means of comparing heparin binding affinities for hLtn variant proteins, heparin-albumin conjugate (Sigma, heparin average molecular weight of 11,000) was immobilized through protein amino groups using standard *N*-hydroxysuccinimide ester/carbodiimide coupling chemistry on a carboxymethyl (C1) sensor chip as described previously (35). Successful immobilization was confirmed by the observation of a ~300 response unit increase. The control flow cell was prepared by immobilizing bovine serum albumin using a similar coupling procedure. This sensor surface displayed minimal nonspecific binding, and a series of hLtn mutants were analyzed at 10 °C in 20 mM sodium phosphate (pH 6), 200 mM NaCl, identical to solution conditions used for NMR analysis of the hLtn structure (4) and heparin binding as described below.

TABLE I
Kinetic parameters for interaction between hLtn mutant protein and surface-immobilized heparin-albumin at 10 °C in 20 mM sodium phosphate (pH 6) 200 mM NaCl

hLtn	k_{on}	k_{off}	K_D	Fold change versus wild-type hLtn
	$M^{-1}\ s^{-1}$	s^{-1}	M	
Wild-type	2.8×10^4	5.8×10^{-4}	21 ± 27	1.0
R18A	2.4×10^4	4.7×10^{-4}	19 ± 22	0.95
R23A	310	2.9×10^{-4}	950 ± 83	47.5
K25A	3.6×10^4	5.4×10^{-4}	15 ± 9	0.75
R43A	383	3.1×10^{-4}	820 ± 124	41
R43A/R23A	342	2×10^{-3}	5800 ± 2100	290
K46S	2.7×10^4	2.8×10^{-4}	11 ± 22	0.55
R61A	1.3×10^4	3.1×10^{-4}	24 ± 19	1.2
R65S	2.1×10^4	6.3×10^{-4}	30 ± 9	1.5
K66A	1.3×10^4	5.3×10^{-4}	42 ± 21	2.1
R70A	2×10^4	4.5×10^{-4}	23 ± 14	1.2

NMR Spectroscopy—NMR experiments were performed on a Bruker DRX600 spectrometer equipped with a $^1H/^{15}N/^{13}C$ CryoProbe®. NMR samples containing 0.25 mM hLtn were prepared in 90% H_2O, 10% D_2O containing 20 mM sodium phosphate (pH 6.0), 200 mM sodium chloride, 0.02% sodium azide. All two-dimensional ^{15}N-^1H HSQC spectra (36) were collected at 10 °C, with spectral widths of 10,000 (^1H) and 2,000 (^{15}N) Hz, using 16 transients per free-induction decay, 200 complex points in the ^{15}N dimension, and 1024 complex points in the ^1H dimension. Total experiment time for each spectrum was 2 h. Heparin titrations were performed by adding substoichiometric aliquots from concentrated stock solutions (10 mg/ml, determined from heparin dry weight) in H_2O of the purified tetra-, hexa-, or decasaccharide described above (33) or a synthetic heparin pentasaccharide corresponding to the antithrombin III binding site of heparin (α-D-GlcNS6S-(1→4)-α-D-GlcA-(1→4)-α-D-GlcNS3S6S-(1→4)-α-L-IdoA2S-(1→4)-α-D-GlcNS6SOMe) (34). Each addition of heparin was monitored by one- and two-dimensional NMR. Chemical shift assignments for the fast-exchange hLtn-pentasaccharide complex were transferred by inspection from the free protein (4) (BioMagResBank ID 5042), because shifts for most resonances could be followed through the course of the titration. A three-dimensional ^{15}N NOESY-HQSC spectrum was used to confirm assignments of the arginine side chain NH resonances and other overlapped signals.

In Vivo Cell Recruitment Assay—Four to 5-week-old female CD-1 mice (Charles River) were anesthetized with isoflurane and injected intraperitoneally with 100 μl of sterile 0.9% sodium chloride solution (Sigma) or 20 μg of various mutants of hLtn diluted in 100 μl of sterile 0.9% sodium chloride solution. At 14 h post-injection, the animals were sacrificed by CO_2 asphyxiation. The peritoneal cavity was washed 3 times with 10 ml of ice-cold phosphate-buffered saline and the total lavage was pooled for individual mice. The total number of cells harvested from each animal was counted using a hematocytometer.

RESULTS AND DISCUSSION

Heparin Binding of Human Lymphotactin—Lymphotactin binds heparin, like most chemokines (13). We monitored the kinetics of the interaction between immobilized hLtn and semi-purified heparin (M_r ~ 11,000) by SPR and obtained an equilibrium dissociation constant (K_d) of 5 nM at 25 °C in 20 mM sodium phosphate (pH 6) (data not shown). Because chemokine-GAG interactions have not been characterized structurally, we sought to form a soluble complex that could be studied by NMR. Addition of semi-purified heparin (M_r ~ 3,000–5,000) to a sample of 0.25 mM hLtn produced an insoluble precipitate, so we used SPR to measure the binding of a series of seven smaller purified heparin fragments ranging from 4 to 20 residues. K_d values for the structurally defined heparin oligosaccharides ranged from 350 nM (ecosisaccharide) to 23 μM (tetrasaccharide) (data not shown), leading us to speculate that one or more of the shorter heparin sequences might bind hLtn in a manner suitable for NMR analysis.

Our previous work showed that hLtn adopts the canonical chemokine fold as a monomer (Fig. 1*a*) at low temperature

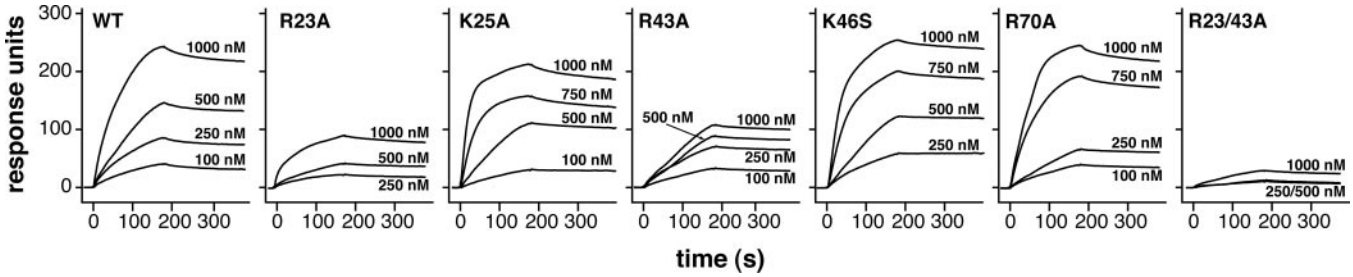

FIG. 3. **SPR analysis of heparin binding.** Sensorgrams are shown for wild-type hLtn, the R23A, K25A, R43A, K46S, and R70A single mutants, and the R23A/R43A double mutant. Association/dissociation kinetics parameters were obtained from simultaneous fitting of multiple injections of each mutant at varying concentrations. Protein concentrations ranged from 100 nM to 2 μM.

(10 °C) in 200 mM NaCl (4), and we recently reported that the protein is conformationally heterogeneous under near-physiological solution conditions (37). The normal chemokine structure interchanges reversibly with a novel conformational state that predominates at elevated temperature (~40 °C) in low salt, however, the functional consequences of this rearrangement are unknown. At physiological solution conditions (37 °C, 150 mM NaCl), the two structural species are present in equal proportions, as detected by two-dimensional NMR, so it is impossible to infer which is more physiologically relevant from biophysical analysis alone. Because the low temperature state is structurally homologous to dozens of other chemokines with known biological activity, and the novel high temperature state has no structural or functional analog, we hypothesize that, whereas each may have a functional role, the chemokine-like conformation of lymphotactin is very likely to be important for *in vivo* activity. To consistently promote the chemokine-like conformation throughout our subsequent studies, we performed all NMR and SPR analyses at 10 °C in 20 mM sodium phosphate buffer with 200 mM NaCl at pH 6.

The Glycosaminoglycan Binding Surface of hLtn—We used two-dimensional NMR to screen a panel of homogenous, structurally defined heparin fragments (tetra-, penta-, hexa-, and decasaccharide) (33, 34) in the solution conditions used for determination of the chemokine-like hLtn conformation (10 °C, 200 mM sodium chloride, 20 mM phosphate, pH 6.0). Addition of substoichiometric amounts of either the deca- or hexasaccharide fragments to submillimolar concentrations of hLtn (200–450 μM) (oligosaccharide:hLtn molar ratio of 1:5) resulted in immediate precipitation and a quantitative reduction in NMR signal intensity consistent with the formation of insoluble complexes. No shifting of the residual protein resonances was detected. Efforts to discourage the precipitation reaction, including lower protein concentration, higher salt, and a wide range of temperature and pH values, were unsuccessful. In contrast, addition of a 2-fold molar excess of the tetrasaccharide under the same solution conditions produced neither insoluble precipitate nor spectral changes, suggesting that the GAG binding site of hLtn requires at least five carbohydrate residues to form a specific complex.

We tested this hypothesis by performing another titration using a synthetic heparin pentasaccharide (34). Comparison of ^{15}N-^{1}H HSQC spectra before and after addition of the pentasaccharide (Fig. 2*a*) revealed chemical shift perturbations for a unique set of residues of hLtn, including a subset of the Arg side chain NH signals (Fig. 2*b*). As increasing amounts of heparin pentasaccharide were added, signals from these residues shifted in a concentration-dependent manner (Fig. 2*c*), demonstrating that the binding reaction occurs in the fast exchange regime of the NMR chemical shift time scale. From these data, it appears that the pentasaccharide binds hLtn with low affinity (K_d ~100 μM) relative to values obtained by SPR using a series of purified heparin oligosaccharides (0.4–23

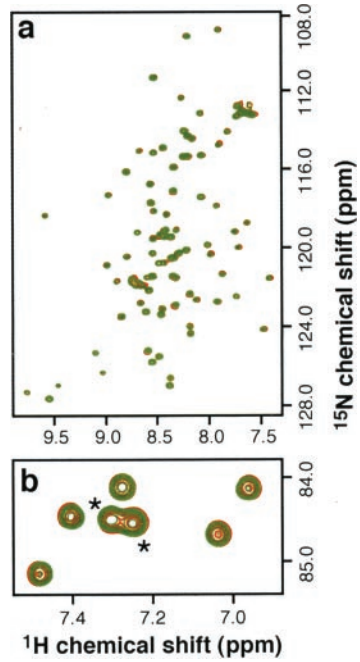

FIG. 4. **R23A/R43A hLtn does not bind heparin.** *a*, two-dimensional ^{1}H-^{15}N HSQC spectrum of R23A/R43A hLtn (0.25 mM) in the presence (*green contours*) and absence (*orange contours*) of a heparin decasaccharide. Spectra were acquired at 10 °C, in 20 mM sodium phosphate (pH 6), 200 mM NaCl. *b*, signals for Arg-23 and Arg-43 are absent (*asterisks*) from the arginine side chain NH region of HSQC spectra of the double mutant. No spectral changes or insoluble precipitate resulted from the addition of heparin.

μM). However, the earlier SPR experiments were performed in the absence of salt at 25 °C, and pentasaccharide binding was not measured so a direct comparison with NMR is not possible. Thus, formation of a high affinity 1:1 hLtn-heparin complex requires a minimal GAG element of six or more carbohydrate residues, and longer heparin chains may promote hLtn oligomerization as suggested for other chemokines (38). However, the limited solubility we observed for complexes with longer heparin oligosaccharides makes them intractable for structural analysis. Despite its low binding affinity, the heparin pentasaccharide is likely to target the GAG recognition elements most important for hLtn activity *in vivo*. We therefore analyzed the NMR titration of this weak but specific complex to identify residues of the chemokine that form the heparin binding site.

Three-dimensional structures determined for a variety of chemokines display the same tertiary structure, comprised of a three-stranded antiparallel β-sheet and C-terminal α-helix. Basic side chains are often the primary mediators of GAG binding, because of favorable electrostatic interactions with the negatively charge sulfate groups. Heparin binding sites identified in other chemokines utilize different combinations of

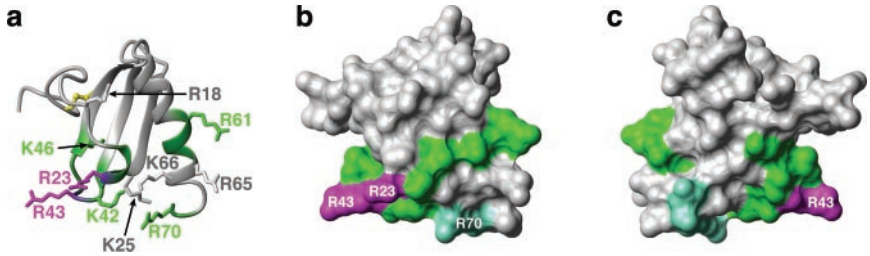

FIG. 5. **Chemical shift changes and SPR results mapped onto the molecular surface of hLtn.** *a*, ribbon diagram of hLtn (Protein Data Bank code 1J9O) with side chains of the mutated basic residues shown. Residues shown in *green* had chemical shift changes greater than 0.035 and no effect on heparin binding affinity. Residues shown in *magenta* had chemical shift changes greater than 0.035 and affected heparin binding affinity. Residues shown in *gray* were not perturbed. *b*, surface representation of hLtn oriented as in the ribbon diagram and colored accordingly, with the exception of Arg-70, shown in *cyan* because it is located in the disordered C-terminal extension and is not precisely positioned in the hLtn structure (4). *c*, heparin interaction surface as in *b* rotated by 180° about the vertical axis. Residues of the unstructured C terminus (71–93) are omitted for clarity.

basic residues near the short 3_{10} helix (20's loop), in the β2–β3 (40's) loop, and in the C-terminal helix (27), whereas unstructured N-terminal residues and the β1–β2 (30's) loop have been implicated as possible determinants in chemokine receptor recognition (39).

Chemical shift perturbations for backbone ^{1}H and ^{15}N resonances in hLtn (Fig. 2*d*) highlight four regions of the hLtn sequence that are affected by the presence of pentasaccharide including the 3_{10} helix preceding β-strand 1, the β2–β3 (40's) loop, residues 62–64 of the C-terminal helix, and residues 70–72. Whereas these regions are distant in primary sequence, they cluster to define a potential GAG interaction surface on the three-dimensional structure (Fig. 2*e*). From inspection of the hLtn sequence, a number of Lys and Arg residues were identified in the vicinity of residues that display shift perturbations: Arg-18, Arg-23, Lys-25, Lys-42, Arg-43, Lys-46, Arg-61, Arg-65, Lys-66, and Arg-70. Arginine side chains possess an amino group that gives rise to an observable signal in the ^{15}N-^{1}H HSQC spectra. Two of the nine arginine side chains in hLtn, Arg-23 and Arg-43, respond noticeably to the titration with heparin (Fig. 2*b*), and these residues are located within segments of the hLtn backbone perturbed by pentasaccharide (Fig. 2*d*). We used these results to guide a mutagenesis study designed to disrupt hLtn-GAG binding.

In Vitro Analysis of Heparin Binding Residues—Each of the 10 basic residues identified from chemical shift perturbations was individually changed to alanine by site-directed mutagenesis. We confirmed proper folding of each mutant by comparing NMR spectra of the wild-type and variant proteins. Each Lys → Ala or Arg → Ala mutant retained the hLtn tertiary fold with three exceptions. None of a series of Lys-42 substitutions (Ala, Ser, and Ile) produced a correctly folded protein based on NMR analysis. Inspection of the NMR structure of hLtn led us to conclude that disruption of hydrophobic contacts involving Lys-42 destabilized the tertiary structure, and that we would be unable to test its role in heparin binding by this approach. The K46A and R65A proteins also displayed altered folding behavior, but a second version of each, K46S and R65S, was prepared. Both proteins folded normally and were used in subsequent analyses.

Kinetic parameters of binding to immobilized albumin-heparin were measured by SPR for each of the hLtn variants at 10 °C in buffer conditions matched to our NMR studies (20 mM phosphate buffer, pH 6, 200 mM NaCl). Most of the substitutions, including R18A, K25A, K46S, R61A, R65S, K66A, and R70A, had little or no effect on the affinity for heparin, displaying equilibrium dissociation constants within a factor of 2 of wild-type hLtn (K_d = 20 nM) (Table I). Strikingly, binding affinities of both the R23A and R43A proteins were reduced by a factor of more than 40, with the differences evident in the SPR sensorgrams (Fig. 3). Based on these results, we produced

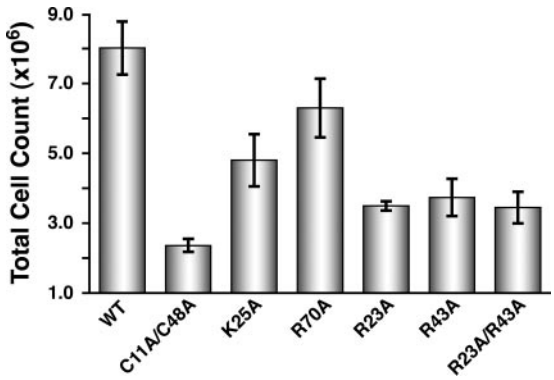

FIG. 6. **hLtn mutants with altered heparin binding are less potent chemoattractants for leukocytes *in vivo*.** hLtn and a series of mutants were tested for their ability to recruit cells into the intraperitoneal cavity of mice. Each protein (20 μg) was injected into the intraperitoneal cavity of 4–5-week-old female CD-1 mice in 100 μl of 0.9% saline, followed by incubation and saline lavage to recover cells responding to the chemoattractant. Cell counts are shown for wild-type hLtn, the R23A, K25A, R43A, and R70A single mutants, and the R23A/R43A double mutant and represent the average from at least five animals. The C11A/C48A mutant (negative control) lacks the stabilizing disulfide bond and is completely unfolded.

the R23A/R43A double mutant protein, confirmed its folding by two-dimensional NMR (Fig. 4), and monitored its interaction with heparin by SPR (Fig. 3). The R23A and R43A mutations combined to reduce the affinity for heparin 300-fold (K_d = 6 μM) relative to wild-type hLtn (Table I). As an independent assessment of relative heparin binding affinities, we eluted all 10 mutant proteins from a heparin-Sepharose column using a linear sodium chloride gradient. In this assay, longer retention times are correlated with increased binding affinities. All proteins eluted in the order predicted by the K_d values shown in Table I (data not shown).

Titration of the R23A/R43A double mutant protein with heparin decasaccharide produced neither insoluble precipitate nor chemical shift perturbations in ^{15}N-^{1}H HSQC spectra (Fig. 4), confirming that the heparin binding site had been disrupted. Fig. 5 highlights residues shown to be central to GAG binding, as determined by NMR and SPR, on the hLtn structure, and illustrates a potential heparin binding surface that encompasses a subset of the positively charged side chains. The core of this GAG binding element is comprised of two basic residues, Arg-23 and Arg-43, that are distant in the amino acid sequence but adjoin each other in the hLtn tertiary structure.

In Vivo Activity of hLtn GAG-binding Mutants—Mutagenesis of residues involved in GAG binding of other chemokines has produced proteins that remain fully functional in cell-based *in vitro* assays for chemotaxis (or Ca^{2+}-flux) (27). A more physiologically realistic environment is therefore needed to assess

the functional impact of disrupting the GAG-chemokine complex. Human Ltn has *in vivo* activity in mice as previously demonstrated by recruitment of leukocytes into the intraperitoneal space (40). We have employed this leukocyte recruitment assay to measure *in vivo* activity for a series of hLtn mutants, including three with diminished heparin binding activity. Recombinant wild-type hLtn proved to be a potent leukocyte chemoattractant in mice, and this functional activity is clearly dependent on tertiary structure, because the unfolded C11A/C48A protein failed to recruit significant numbers of cells (Fig. 6). All three proteins with disrupted heparin binding sites, R23A, R43A, and R23A/R43A, showed significantly diminished activity in the *in vivo* recruitment assay when compared with wild-type hLtn. The K25A and R70A mutants, which bind heparin as well as wild-type hLtn (Table I), were functional *in vivo*, although at reduced levels. Whereas this may suggest a secondary role in formation of hLtn-GAG complexes, chemotactic activity would also be diminished if either residue participated in binding or activation of the specific hLtn receptor, XCR1, or stabilized an essential quaternary structure of the chemokine. However, Lys-25, Arg-70, and other positively charged side chains are located near Arg-23 and Arg-43 on the hLtn surface (Fig. 5) and might interact with bound heparin but contribute less to the total energy of the interaction.

Interestingly, whereas heparin affinities for the single mutants R23A and R43A are reduced roughly 40-fold compared with wild-type hLtn, and the R23A/R43A double mutant binds with 300-fold lower affinity, these three proteins were inactivated to an equal degree *in vivo*. Hence, either of the single substitutions at Arg-23 and Arg-43 disrupted hLtn-GAG interactions sufficiently to exceed a threshold beyond which further reductions in heparin binding affinity had no functional effect. These results suggest that even modest disruptions of GAG binding can have dramatic consequences for the formation of active chemokine signaling complexes.

Comparisons with Other Chemokine-GAG Interactions—Where previous analysis of chemokine-GAG interactions have relied on sequence comparisons to direct mutagenic studies, we have pursued a structure-based approach, using NMR to detect the interaction of a heparin oligosaccharide with specific residues of the protein. These residues and others that are located nearby in the three-dimensional structure were then targeted for mutagenesis to gauge their relative contributions to the binding energy. Like many CC chemokines, the 40's loop of hLtn contains a basic cluster (BB*XX*B) that resembles one of the motifs identified as a common heparin binding sequence element. In the cases of RANTES, MIP1-β, and SDF1-α, neutralization of all basic residues within the analogous BB*X*B motif was required to reduce or eliminate GAG binding (18, 19, 22, 23, 41). However, our results showed that, of this cluster of basic residues in hLtn, only Arg-43 contributes significantly to the affinity for heparin.

Whereas a consensus GAG binding site has not been established for the CXC chemokines, mutagenesis studies have implicated a conserved basic residue in the N-loop of PF-4 (Arg-22), IP-10 (Arg-22), and IL-8 (Lys-20) that participates in GAG binding. Other residues critical to GAG binding are found in various locations in these chemokines. For example, the C-terminal helix of PF-4 and IL-8 and the 40's loop of IP-10 each contain basic residues that participate in GAG binding (21, 24, 42). In hLtn, a similarly positioned N-loop residue, Arg-23, plays a key role in GAG binding, whereas mutations of basic residues in the C-terminal helix did not affect heparin affinity.

The hLtn GAG binding surface includes Arg-23 and Arg-43, a unique combination of basic residues that play similar roles in many CXC and CC chemokines, respectively, and illustrates the diversity of GAG binding sites in chemokines. Whereas the chemokines are generally highly basic proteins, the importance of specific GAG binding residues varies among family members. For example, basic residues in the C-terminal helix of MCP-1, a CC chemokine, are critical to GAG binding, whereas the essential residues in other CC chemokines are located in a BB*X*B motif in the 40's loop (20). The lack of a clear consensus GAG binding motif across the chemokine family might suggest that immobilization in the extracellular matrix occurs through degenerate electrostatic forces between polyanionic carbohydrates and highly electropositive protein surfaces. However, our results and previous studies demonstrate that chemokine GAG interactions are highly specific and mediated by key basic residues that are unique for each chemokine.

Conclusions—The T cell chemoattractant lymphotactin contains 15 positively charged amino acids and binds heparin with nanomolar affinity. We used NMR to monitor binding of a synthetic heparin pentasaccharide to hLtn, and identified a glycosaminoglyan recognition surface containing a subset of the basic residues. Our subsequent analysis of binding determinants by mutagenesis, SPR, and *in vivo* activity showed that NMR served as an efficient and reliable method for identifying the elements required for high affinity GAG binding. We hypothesize that, like other chemokines, hLtn function depends on interactions with components of the extracellular matrix, and that high affinity recognition of glycosaminoglycans by this chemokine is specifically mediated by the side chains of Arg-23 and Arg-43.

High-resolution structure determination requires that the biomolecular components be pure and homogeneous. Other NMR studies of chemokine-GAG binding used heterogeneous heparin preparations (42) unsuitable for detailed structural analysis, or purified heparin disaccharides (19, 43), which are unlikely to span a minimal GAG binding site on the chemokine surface. Whereas the heparin pentasaccharide used in this study binds hLtn with low affinity under the conditions used, chemical shift mapping suggest that it interacts with an extensive region of the protein surface. Lymphotactin undergoes a novel reversible structural interconversion that necessarily alters the heparin binding site observed under these conditions. This structural equilibrium can be altered by mutagenesis, and a lymphotactin variant that preferentially adopts only the novel non-chemokine structure displays no leukocyte recruitment activity *in vivo*.[2] These preliminary results lend additional support to our hypothesis that biochemical activities specific to the chemokine-like conformation are essential for lymphotactin function. Our future studies will be directed at understanding the specific functional roles for both structural species of this unusual chemokine.

REFERENCES

1. Keane, M. P., and Strieter, R. M. (2000) *Crit. Care Med.* **28,** N13–N26
2. Zlotnik, A., and Yoshie, O. (2000) *Immunity* **12,** 121–127
3. Gale, L. M., and McColl, S. R. (1999) *Bioessays* **21,** 17–28
4. Kuloglu, E. S., McCaslin, D. R., Kitabwalla, M., Pauza, C. D., Markley, J. L., and Volkman, B. F. (2001) *Biochemistry* **40,** 12486–12496
5. Fernandez, E. J., and Lolis, E. (2002) *Annu. Rev. Pharmacol. Toxicol.* **42,** 469–499
6. Rossi, D., and Zlotnik, A. (2000) *Annu. Rev. Immunol.* **18,** 217–242
7. Proudfoot, A. E. (2002) *Nat. Rev. Immunol.* **2,** 106–115
8. Hedrick, J. A., and Zlotnik, A. (1998) *Clin. Immunol. Immunopathol.* **87,** 218–222
9. Wang, J. D., Nonomura, N., Takahara, S., Li, B. S., Azuma, H., Ichimaru, N., Kokado, Y., Matsumiya, K., Miki, T., Suzuki, S., and Okuyama, A. (1998) *Immunology* **95,** 56–61
10. Middel, P., Thelen, P., Blaschke, S., Polzien, F., Reich, K., Blaschke, V., Wrede, A., Hummel, K. M., Gunawan, B., and Radzun, H. J. (2001) *Am. J. Pathol.* **159,** 1751–1761
11. Blaschke, S., Middel, P., Dorner, B. G., Blaschke, V., Hummel, K. M., Kroczek,

[2] F. C. Peterson, T. J. Nelson, and B. F. Volkman, unpublished results.

R. A., Reich, K., Benoehr, P., Koziolek, M., and Muller, G. A. (2003) *Arthritis Rheum.* **48,** 1858–1872
12. Rousseau, R. F., Haight, A. E., Hirschmann-Jax, C., Yvon, E. S., Rill, D. R., Mei, Z., Smith, S. C., Inman, S., Cooper, K., Alcoser, P., Grilley, B., Gee, A., Popek, E., Davidoff, A., Bowman, L. C., Brenner, M. K., and Strother, D. (2003) *Blood* **101,** 1718–1726
13. Kuschert, G. S., Coulin, F., Power, C. A., Proudfoot, A. E., Hubbard, R. E., Hoogewerf, A. J., and Wells, T. N. (1999) *Biochemistry* **38,** 12959–12968
14. McFadden, G., and Kelvin, D. (1997) *Biochem. Pharmacol.* **54,** 1271–1280
15. Proudfoot, A. E. (1998) *Eur. J. Dermatol.* **8,** 147–157
16. Koopman, W., and Krangel, M. S. (1997) *J. Biol. Chem.* **272,** 10103–10109
17. Laurence, J. S., Blanpain, C., Burgner, J. W., Parmentier, M., and LiWang, P. J. (2000) *Biochemistry* **39,** 3401–3409
18. Koopmann, W., Ediriwickrema, C., and Krangel, M. S. (1999) *J. Immunol.* **163,** 2120–2127
19. Proudfoot, A. E. I., Fritchley, S., Borlat, F., Shaw, J. P., Vilbois, F., Zwahlen, C., Trkola, A., Marchant, D., Clapham, P. R., and Wells, T. N. (2001) *J. Biol. Chem.* **276,** 10620–10626
20. Chakravarty, L., Rogers, L., Quach, T., Breckenridge, S., and Kolattukudy, P. E. (1998) *J. Biol. Chem.* **273,** 29641–29647
21. Kuschert, G. S., Hoogewerf, A. J., Proudfoot, A. E., Chung, C. W., Cooke, R. M., Hubbard, R. E., Wells, T. N., and Sanderson, P. N. (1998) *Biochemistry* **37,** 11193–11201
22. Amara, A., Lorthioir, O., Valenzuela, A., Magerus, A., Thelen, M., Montes, M., Virelizier, J. L., Delepierre, M., Baleux, F., Lortat-Jacob, H., and Arenzana-Seisdedos, F. (1999) *J. Biol. Chem.* **274,** 23916–23925
23. Sadir, R., Baleux, F., Grosdidier, A., Imberty, A., and Lortat-Jacob, H. (2001) *J. Biol. Chem.* **276,** 8288–8296
24. Campanella, G. S., Lee, E. M., Sun, J., and Luster, A. D. (2003) *J. Biol. Chem.* **278,** 17066–17074
25. Cardin, A. D., and Weintraub, H. J. (1989) *Arteriosclerosis* **9,** 21–32
26. Lortat-Jacob, H., Grosdidier, A., and Imberty, A. (2002) *Proc. Natl. Acad. Sci. U. S. A.* **99,** 1229–1234
27. Proudfoot, A. E., Handel, T. M., Johnson, Z., Lau, E. K., LiWang, P., Clark-Lewis, I., Borlat, F., Wells, T. N., and Kosco-Vilbois, M. H. (2003) *Proc. Natl. Acad. Sci. U. S. A.* **100,** 1885–1890
28. Faham, S., Hileman, R. E., Fromm, J. R., Linhardt, R. J., and Rees, D. C. (1996) *Science* **271,** 1116–1120
29. Proudfoot, A. E., Power, C. A., Rommel, C., and Wells, T. N. (2003) *Semin. Immunol.* **15,** 57–65
30. Dougherty, W. G., Cary, S. M., and Parks, T. D. (1989) *Virology* **171,** 356–364
31. Kelner, G., Kennedy, J., Bacon, K., Kleyensteuber, S., Largaespada, D., Jenkins, N., Copeland, N., Bazan, J., Moore, K., Schall, T., and Zlotnik, A. (1994) *Science* **266,** 1395–1399
32. Dorner, B., Müller, S., Entschladen, F., Schröder, J. M., Franke, P., Kraft, R., Friedl, P., Clark-Lewis, I., and Kroczek, R. A. (1997) *J. Biol. Chem.* **272,** 8817–8823
33. Pervin, A., Gallo, C., Jandik, K. A., Han, X. J., and Linhardt, R. J. (1995) *Glycobiology* **5,** 83–95
34. Yu, G., LeBrun, L., Gunay, N. S., Hoppensteadt, D., Walenga, J. M., Fareed, J., and Linhardt, R. J. (2000) *Thromb. Res.* **100,** 549–556
35. Zhang, F., Fath, M., Marks, R., and Linhardt, R. J. (2002) *Anal. Biochem.* **304,** 271–273
36. Mori, S., Abeygunawardana, C., Johnson, M. O., and van Zijl, P. C. (1995) *J. Magn. Reson. Ser. B* **105,** 94–98
37. Kuloglu, E. S., McCaslin, D. R., Markley, J. L., and Volkman, B. F. (2002) *J. Biol. Chem.* **277,** 17863–17870
38. Hoogewerf, A. J., Kuschert, G. S. V., Proudfoot, A. E., Borlat, F., Clark-Lewis, I., Power, C. A., and Wells, T. N. C. (1997) *Biochemistry* **36,** 13570–13578
39. Loetscher, P., and Clark-Lewis, I. (2001) *J. Leukocyte Biol.* **69,** 881–884
40. Hedrick, J. A., Saylor, V., Figueroa, D., Mizoue, L., Xu, Y., Menon, S., Abrams, J., Handel, T., and Zlotnik, A. (1997) *J. Immunol.* **158,** 1533–1540
41. Laurence, J. S., Blanpain, C., Leener, A. D., Parmentier, M., and LiWang, P. J. (2001) *Biochemistry* **40,** 4990–4999
42. Mayo, K. H., Ilyina, E., Roongta, V., Dundas, M., Joseph, J., Lai, C. K., Maione, T., and Daly, T. J. (1995) *Biochem. J.* **312,** 357–365
43. McCornack, M. A., Cassidy, C. K., and LiWang, P. J. (2003) *J. Biol. Chem.* **278,** 1946–1956
44. Koradi, R., Billeter, M., and Wüthrich, K. (1996) *J. Mol. Graphics* **14,** 51–55
45. Grzesiek, S., Bax, A., Clore, G. M., Gronenborn, A. M., Hu, J. S., Kaufman, J., Palmer, I., Stahl, S. J., and Wingfield, P. T. (1996) *Nat. Struct. Biol.* **3,** 340–345
46. Garrett, D. S., Seok, Y. J., Peterkofsky, A., Clore, G. M., and Gronenborn, A. M. (1997) *Biochemistry* **36,** 4393–4398